高出力レーザーと 高エネルギー密度科学

兒玉　了祐

大阪大学大学院工学研究科
レーザーエネルギー学研究センター

高出力レーザーによる高エネルギー密度状態

レーザープラズマの世界
- 非平衡プラズマ
- 輻射と流体
- 超高圧状態
- 超高密度電流
- 粒子加速
- 超高電場、磁場

結語

高出力レーザーで開拓できる高エネルギー密度の状態

レーザーで既に観測されている

100億気圧以上の圧力
1億アンペア以上の超高電流
10億ガウス程度の超高磁場

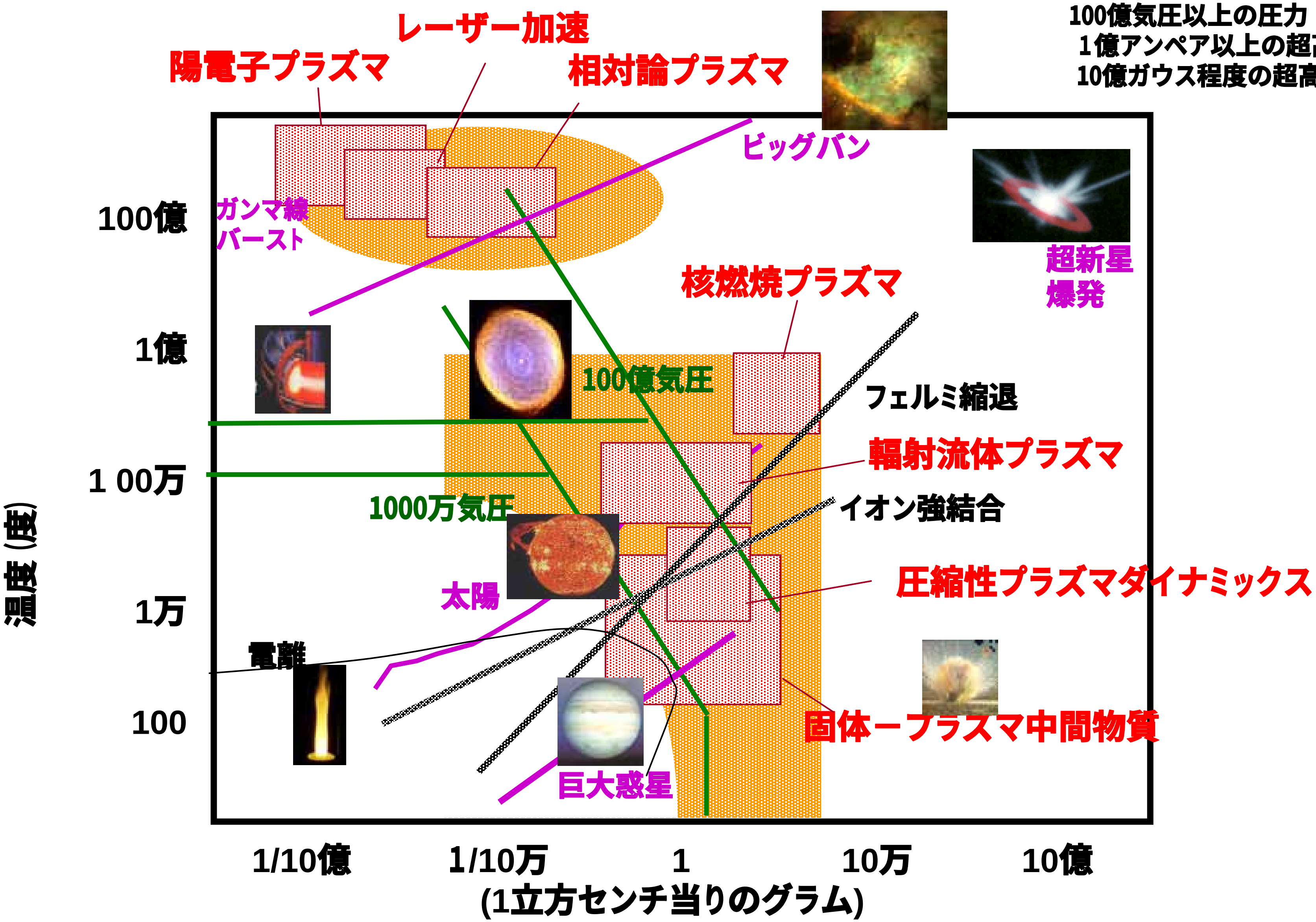

非熱平衡(X線レーザー)
　束縛遷移
　自由－束縛遷移

粒子加速
　イオンジェットと加熱
　長尺ジェット
　電子加速

輻射と流体
　輻射流体ジェット
　輻射衝撃波

超高密度電流
　不安定性と安定化
　伝播自己組織化
　電子流ジェット

レーザー技術
プラズマ制御技術

超高圧・高密度
　衝撃波
　爆縮
　定容加熱

超高電場・磁場
　電場発生
　磁場計測

無衝突衝撃波
　光子圧力による衝撃波
　衝撃波加速

非平衡プラズマからのX線輻射： X線レーザー

束縛電子の非平衡

電子衝突励起	1987年発振 現在応用
再結合励起	不安定性 (未だ制御できていない)
光電離励起	有望視され続けて実現できていない
内殻励起	実証

自由束縛電子の非平衡

X線レーザー励起	プラズマでは理論のみ

非平衡電子分布(non Maxwell 電子による輻射、
非等方分布電子による偏光)

X-ray Laser was already Demonstrated in a Laboratory with Intense Lasers

D. Matthews et al., J. Opt. Soc. Am. B 4, 575-587 (1987)

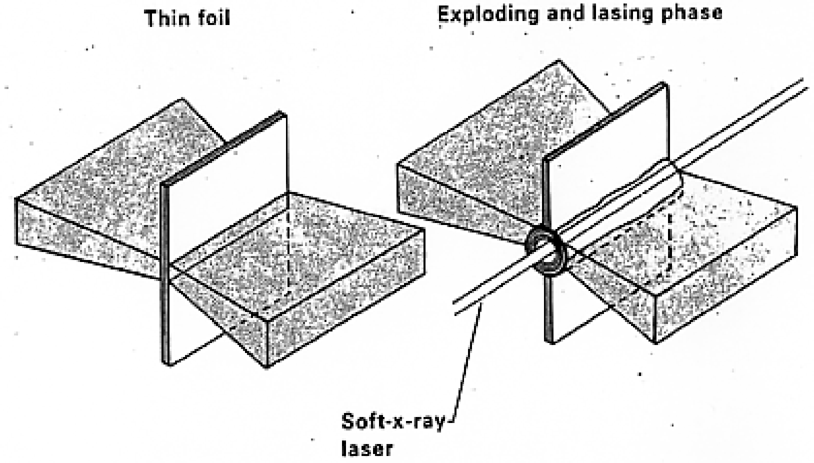

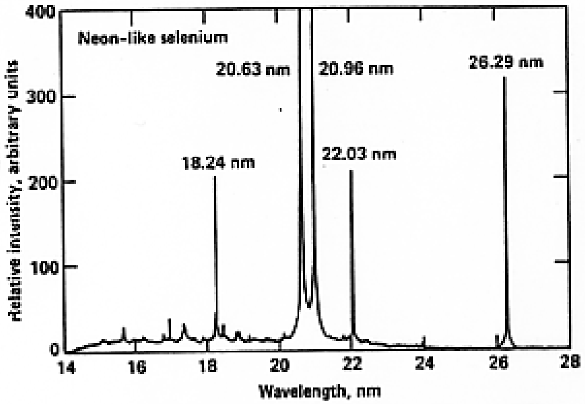

Fig. 5. Ne-like Se x-ray laser spectrum using a 2-cm amplifier. 20.63- and 20.96-nm lines are not to scale; they are deliberately overexposed to show weaker lines.

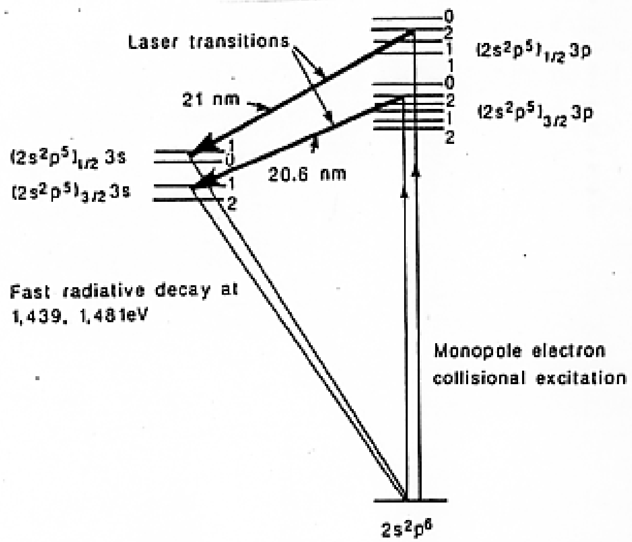

Fig. 4 Energy-level structure of Se^{24+}, after D. L. L. Matthews

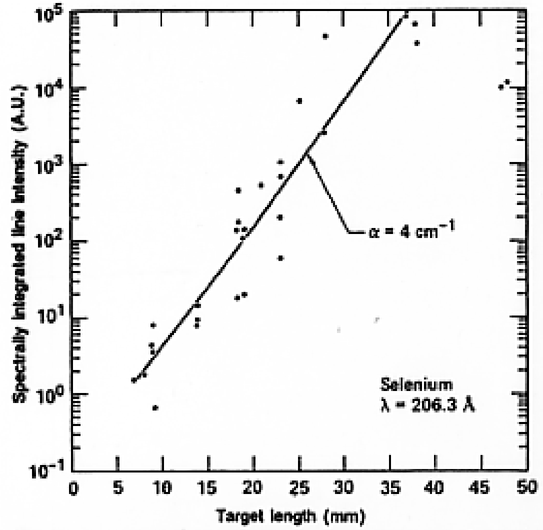

Fig. 6. Intensity versus amplifier length curve for the $J = 2$ to 1 transition at 10.63 nm for Ne-like Se. A solid curve is also shown exhibiting the intensity scaling with length, assuming a gain coefficient of 4 cm^{-1}. A.U., arbitrary units.

Stimulated Free-Bound Emission from X-ray Laser Pumped Plasma
Phys. Rev. Lett. 69, (1992) 77 R Kodama

光励起非平衡（自由ー束縛間）

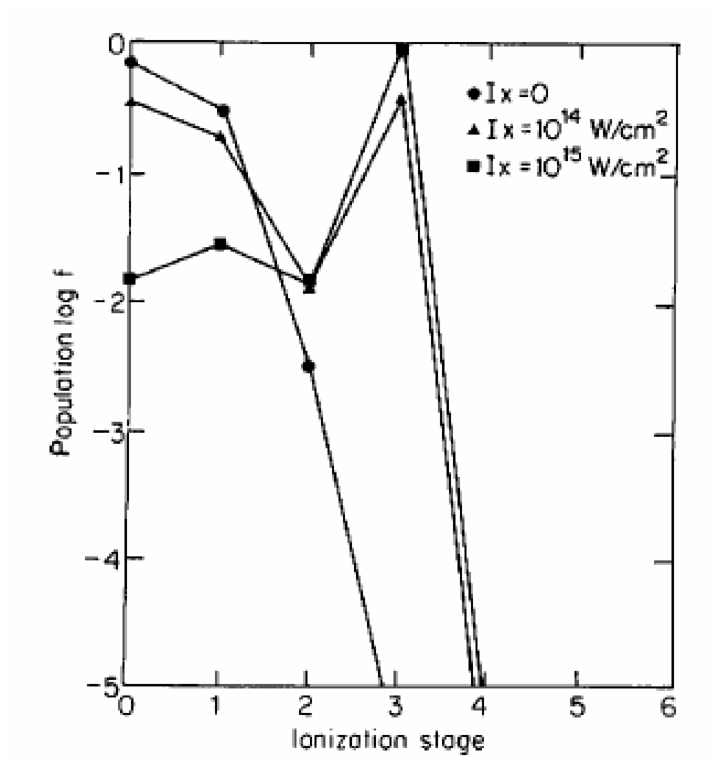

FIGURE 2. Charge-state abundance in C plasmas as a function of the incident X-ray laser intensity with a wavelength of 23 nm at a fixed electron temperature of 5 eV and electron density of 10^{22} cm^{-3}.

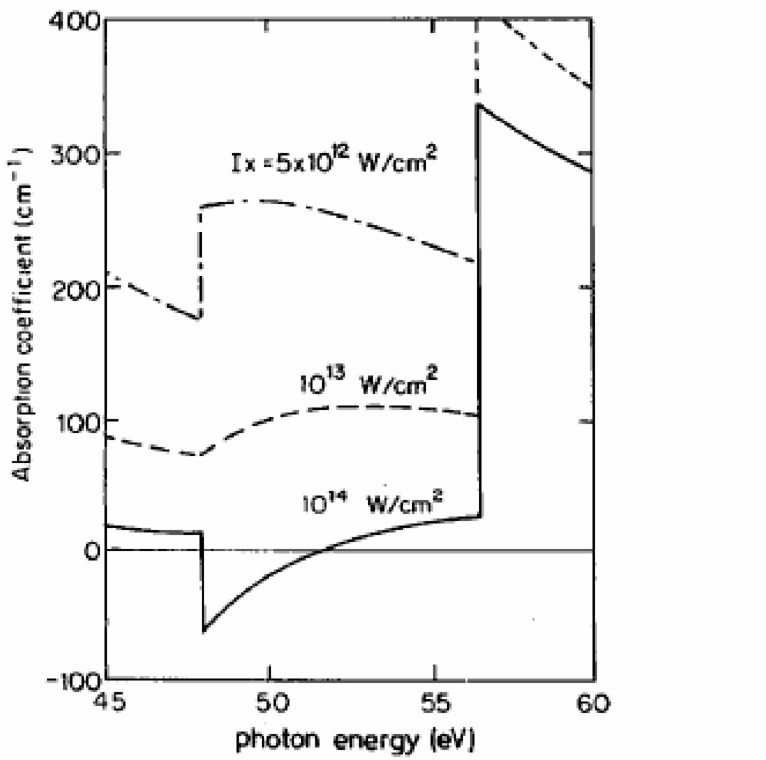

FIG. 1. Absorption spectra (45–60 eV) in carbon plasmas at $T_e = 5$ eV and $N_e = 2\times10^{21}$ cm^{-3} as a function of the 23 nm (54 eV) x-ray laser intensity.

非熱平衡(X線レーザー)
- 束縛遷移
- 自由－束縛遷移

粒子加速
- イオンジェットと加熱
- 長尺ジェット
- 電子加速

輻射と流体
- 輻射流体ジェット
- 輻射衝撃波

超高密度電流
- 不安定性と安定化
- 伝播自己組織化
- 電子流ジェット

レーザー技術
プラズマ制御技術

超高圧・高密度
- 衝撃波
- 爆縮
- 定容加熱

超高電場・磁場
- 電場発生
- 磁場計測

無衝突衝撃波
- 光子圧力による衝撃波
- 衝撃波加速

Experiments on the Radiative Jet with the GEKKOXII Laser

ILE Osaka Univ.

target

material : CH, Al, Fe, Au
diameter : 1600 μm
ipen angle : 120deg

Laser

pulse duration : 100 ps、
wavelength : 0.53 μm
energy : 500J
Intensity : $2x10^{14}$ W /cm ^{2}

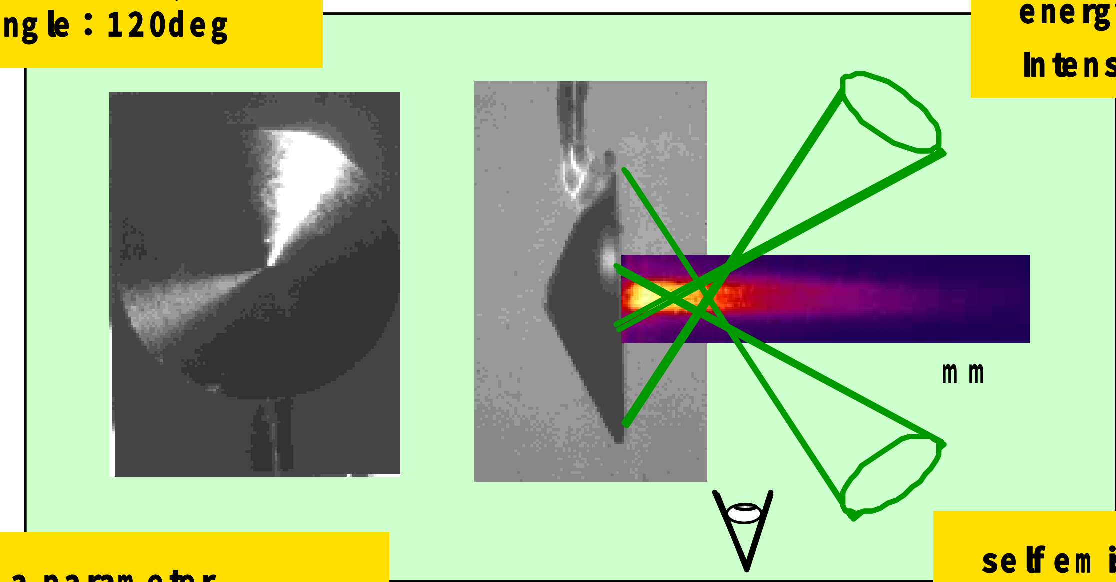

Plasma parameter

Electron Temp.:
a few 100eV-a few keV
density : 0.0001-0.1 g/cc

self emission image
shadow image
x-ray spectroscopy

X-ray emissions at same timing (1.3 ns after the laser irradiation) suggest that diameter of jets increases with decreasing atomic number of the target

ILE Osaka Univ.

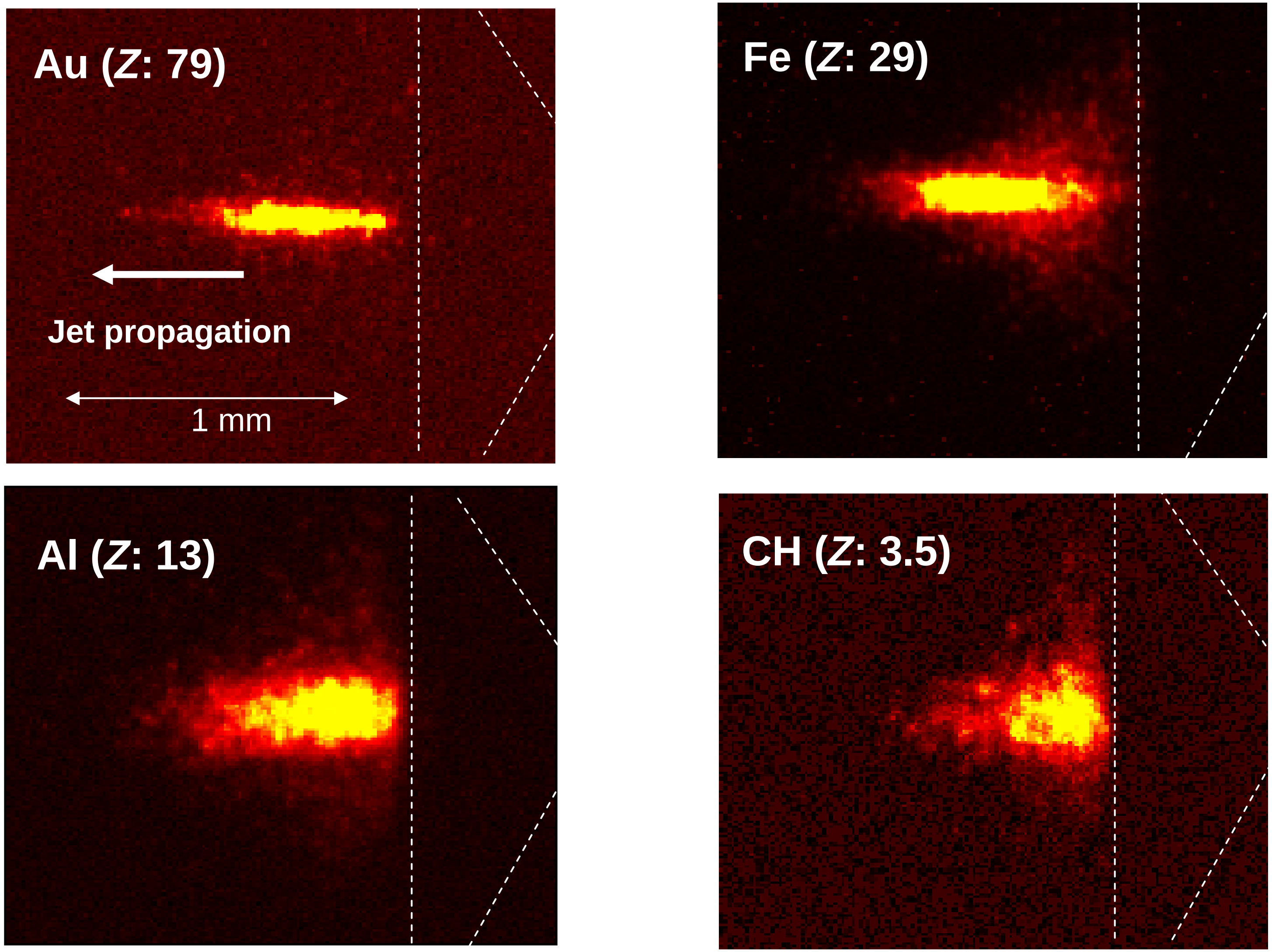

Radiation cooling time and the jet radius well correlate with <*Z*>

ILE Osaka Univ.

Lineouts of normalized self-emission

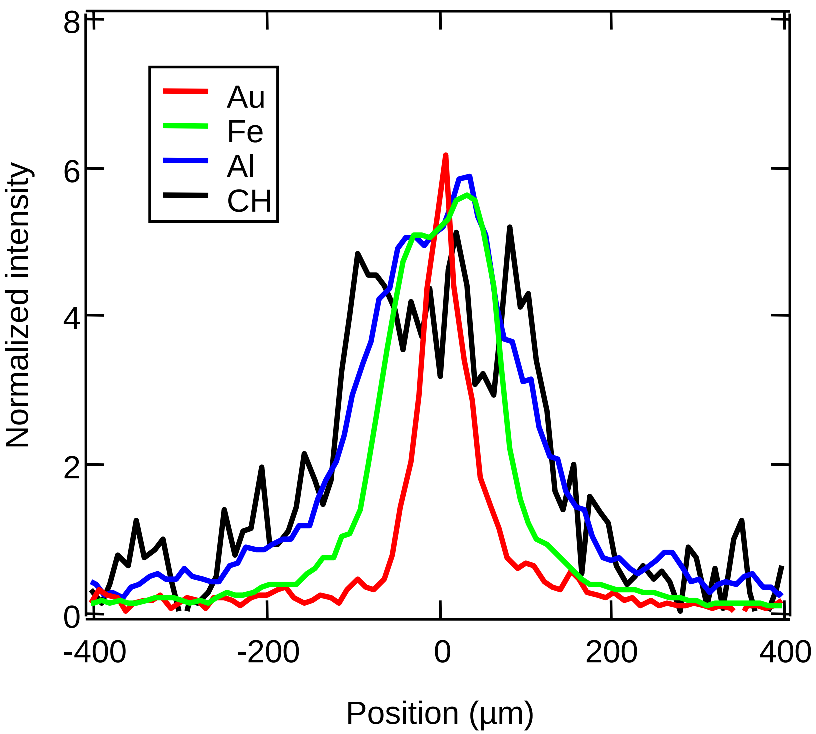

Jet radius and radiation cooling time* vs. <*Z*>

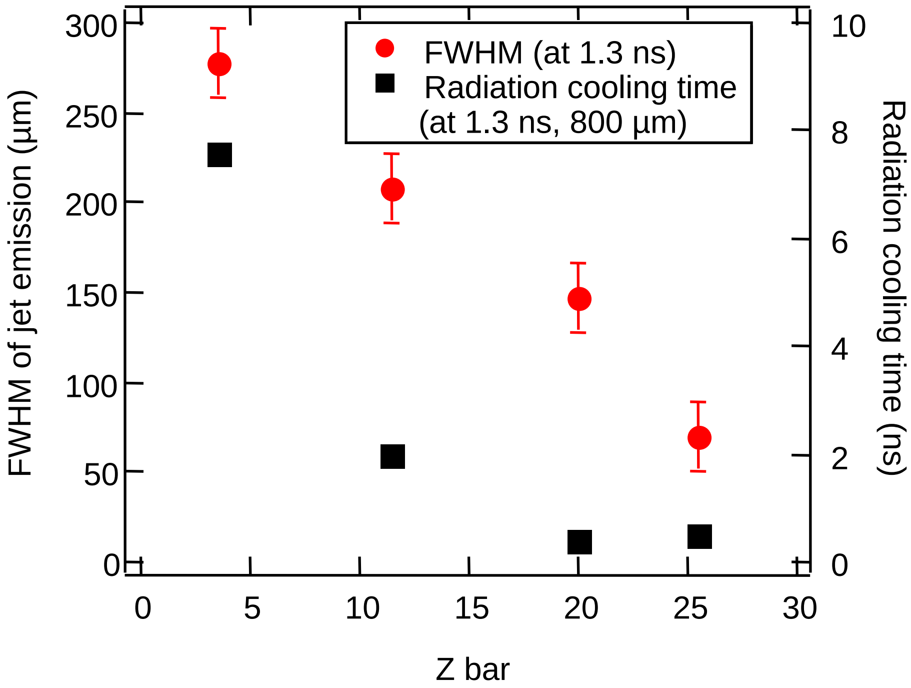

*Radiation cooling time is by calculated parameters from LASNEX-2D simulation

Radiation cooling time τ_c

$$\tau_c = \varepsilon_k / q_{rad}$$

ε_k: **Energy density**

q_{rad} : **Radiation flux**

Summary

We have observed radiative cooling effect of high-Mach number jets of astrophysical interest

ILE Osaka Univ.

Dimensionless terms in astrophysical jets and our jets*

	Astrophysical jets (HH)	Au jet	Fejet	Al jet	CH jet
M	10 - 20	10 - 50	10 - 40	5 - 15	2 - 8
χ	0.1 - 10	~ 2	~ 2	~ 7	~ 30
η	1 - 10	>>1000			

$\chi = v_{jet} \cdot \tau_{rad} / R_{jet}$

$\eta = \rho_{jet} / \rho_{ambient}$

- **Our experimental results suggest that the radiative cooling effect is very essential for generation of well-collimated high-density outflow.**
- **The radiative cooling effect is a function of atomic number of the target (or ionization state <*Z*>). High-*Z* jets (Au, Fe) are "radiative jets", and low-z jets (Al, CH) are apparently near "adiabatic jets".**
- **Calculations from LASNEX-2D simulation well reproduce the experimental results. The calculations show the radiative collapse for high-Z jet.**
- **The radiative effect is sensitive to its radiation cooling time vs. its hydrodynamics time.**
- **The dimensionless terms in our jets are relevant to those of astrophysical jets except for the density ratio η. This should be improved using foam (or gas-bag) targets.**

Several efforts are done to create radiative blast wave with intense lasers

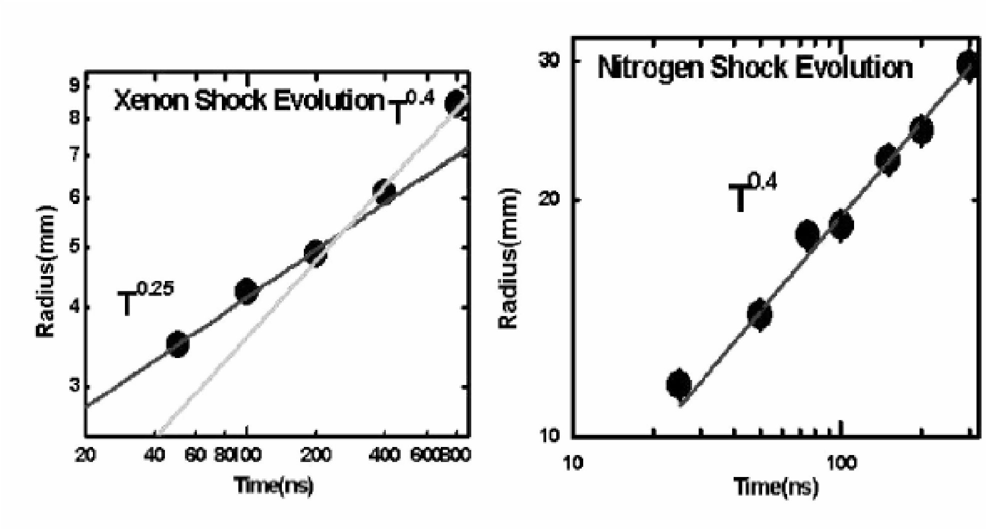

FIG. 2. Blast wave trajectory through xenon and nitrogen gas. After ~200 ns in xenon the trajectory changes from $t^{0.25}$, indicative of a highly radiative blast wave, to $t^{0.4}$, consistent with the energy conserving Taylor–Sedov solution. The nitrogen blast wave trajectory is always consistent with the Taylor–Sedov solution. The error bars are smaller than the data points.

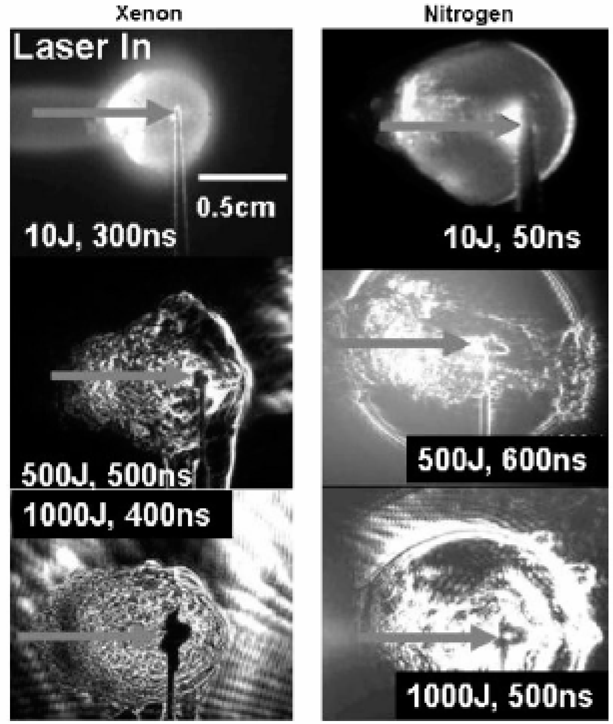

FIG. 3. Dark-field images of blast waves traveling through xenon (left) and nitrogen (right) gas produced by various drive laser energies. In all cases drive laser enters from left. From top to bottom drive laser energies are ~10, ~500, and ~1000 J. There is a contrast both in the small scale structure and the laser-side feature between the gases.

A. D. Edens et al., Phys. Plasmas 11, 4968 (2004)

Radiative blast wave propagates more slower than “classical” blast wave

Classical blast wave is solved by mass, momentum, and energy conservation with thin shell approximation (+ Rankine - Hugoniot relationships).

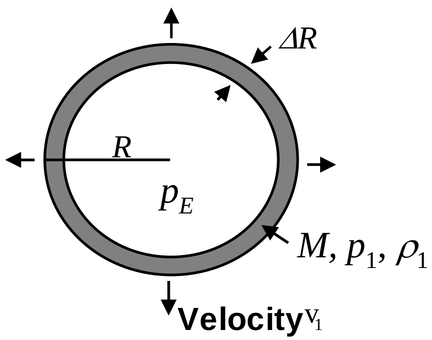

Mass conservation $\pi R^2 \ell \rho_0 = 2\pi R \ell \Delta R \rho_1$

ℓ: length of cylinder

α: constant

Momentum conservation $\frac{d}{dt}(Mv_1) = 2\pi R \ell p_E = 2\pi R \ell \alpha p_1$

Kinetic energy, Thermal energy $E_k = \frac{1}{2} M v_1^2 \quad E_T = \frac{\alpha p_1}{\gamma - 1} \pi R^2 \ell$

Shell trajectory $R = \left\{ \frac{4}{\pi} \frac{(\gamma-1)(\gamma+1)^2}{3\gamma-1} \right\}^{\frac{1}{4}} \left(\frac{E_0}{\rho_0 \ell} \right)^{\frac{1}{4}} t^{\frac{1}{2}}$

Strong radiative blast wave is solved by momentum conservation because of radiative cooling

Momentum conservation $\pi R^2 \rho_0 \dot{R} = \pi R_0^2 \rho_0 \dot{R}_0$

Shell trajectory $R = \left(\frac{18 E_0 d_0^2}{\pi \rho_0} \right)^{\frac{1}{6}} t^{\frac{1}{3}}$

Previous work suggest thin-shelled instabilities can arrive in spherical geometry when $\gamma < 1.2$

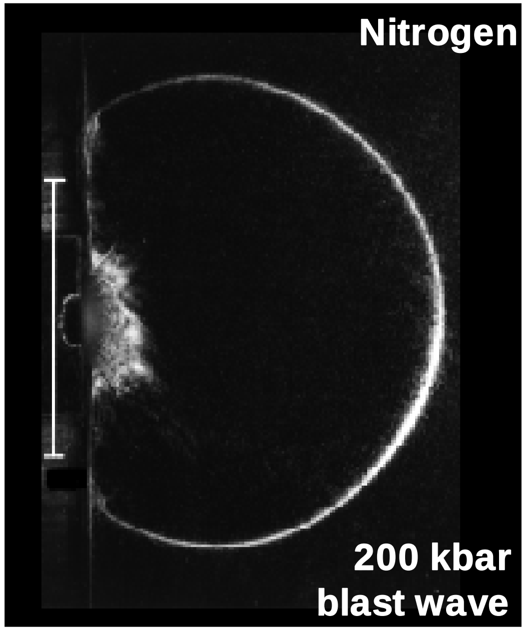

Blast wave in nitrogen gas is stable

Blast wave in xenon gas is unstable

J. Grun *et al.*,
Phys. Rev. Lett. 66, 2738 (1991)

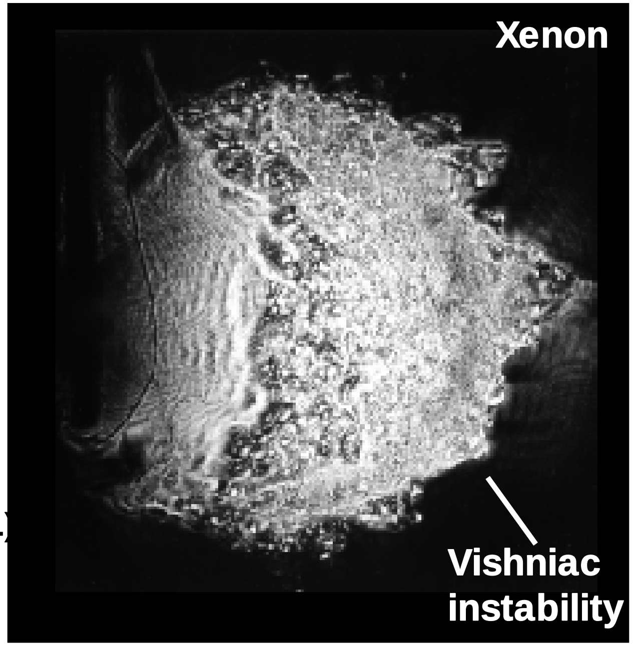

非熱平衡(X線レーザー)
束縛遷移
自由－束縛遷移

粒子加速
イオンジェットと加熱
長尺ジェット
電子加速

輻射と流体
輻射流体ジェット
輻射衝撃波

超高密度電流
不安定性と安定化
伝播自己組織化
電子流ジェット

レーザー技術
プラズマ制御技術

超高圧・高密度
衝撃波
爆縮
定容加熱

超高電場・磁場
電場発生
磁場計測

無衝突衝撃波
光子圧力による衝撃波
衝撃波加速

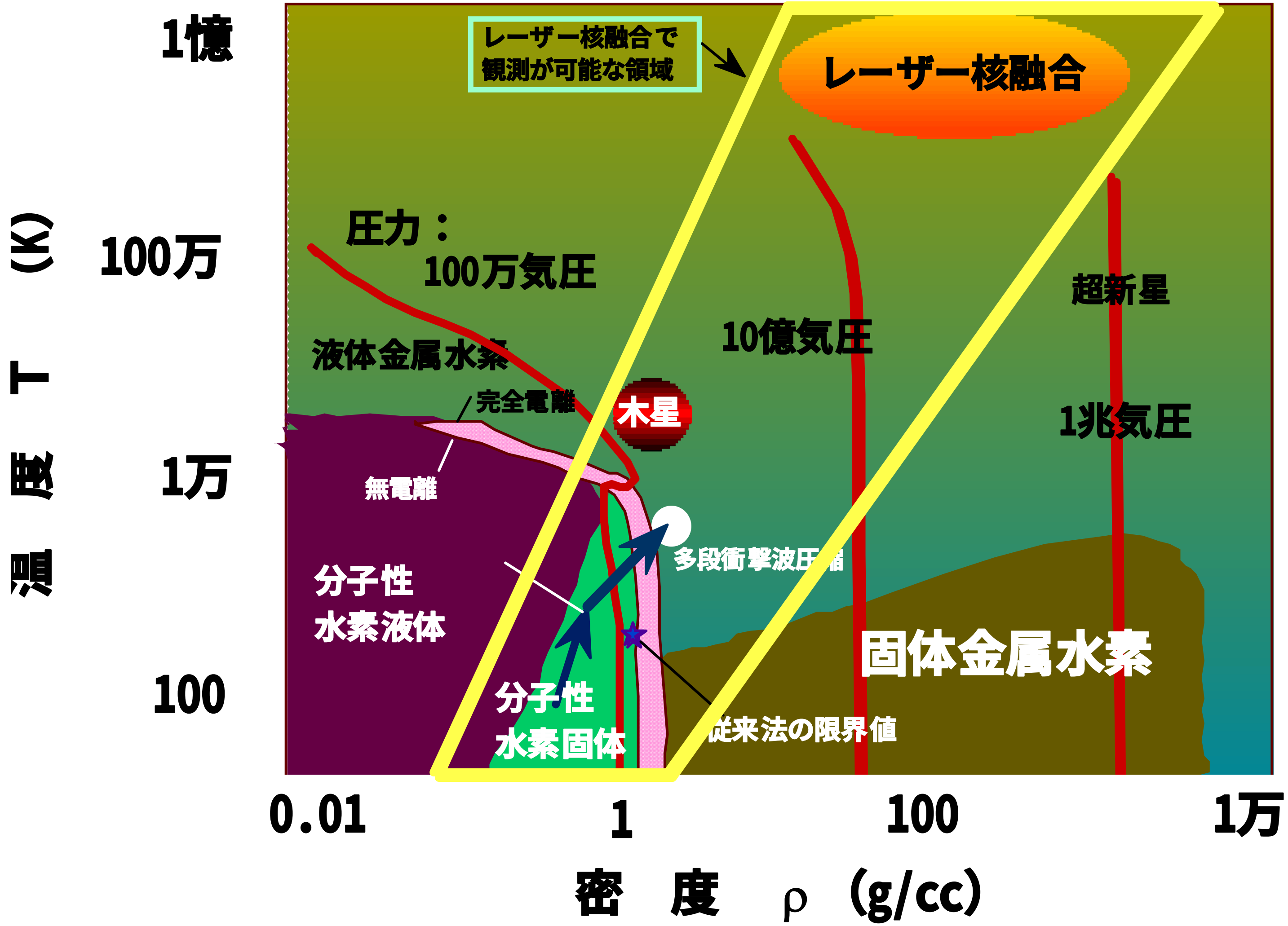

1億
100万
1万
100
温 度 T (K)
レーザー核融合で
観測が可能な領域
レーザー核融合
圧力：
100万気圧
10億気圧
超新星
1兆気圧
液体金属水素
完全電離
木星
無電離
多段衝撃波圧
分子性
水素液体
分子性
水素固体
固体金属水素
従来法の限界値
0.01
1
100
1万
密 度 ρ (g/cc)

Diamond under high pressure (over 10Mbar region) and low temperature will transform to metallic phase.

ILE OSAKA

Previous theoretical investigation is suggested that diamond will transform to metallic phase of BC8 or bct-4 crystal structure.

Reference. D.A. Young and R. Grover, Shock Wave In Condnsed Matter 131 (1988)

Diamond will transform to liquid phase under 10Mbar region by single-shock compression. Low-entropy is required for the metallization of diamond.

Diamond Structure

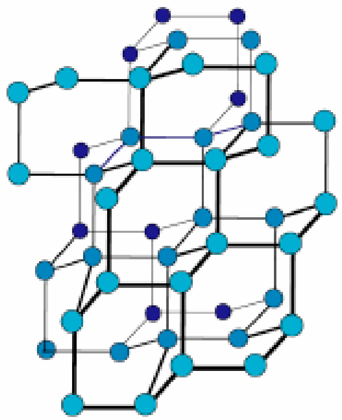

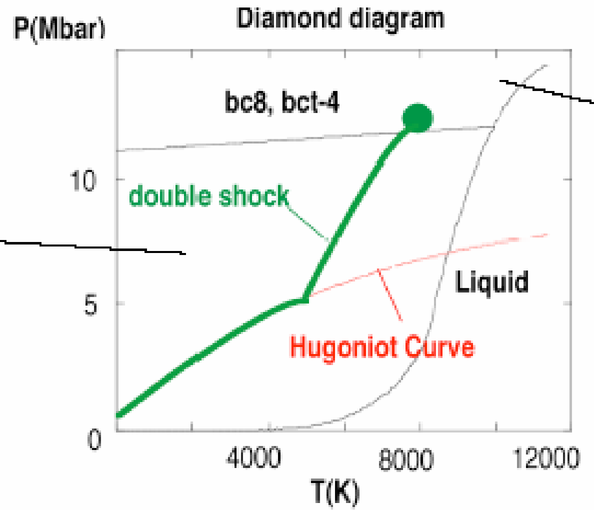

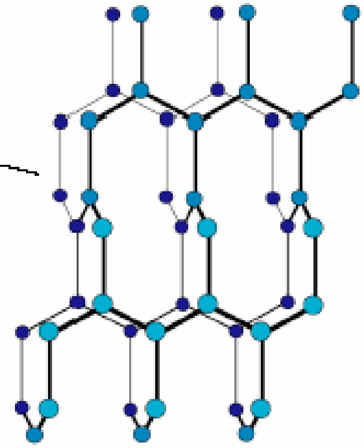

bct-4 Structure

We have demonstrated a preliminary experiment on metallization of diamond by high power laser to reach 10Mbar region.

The ILESTA 1D-simulation indicates that diamond is compressed to the metallic-phase by impedance mismatching technique.

ILE OSAKA

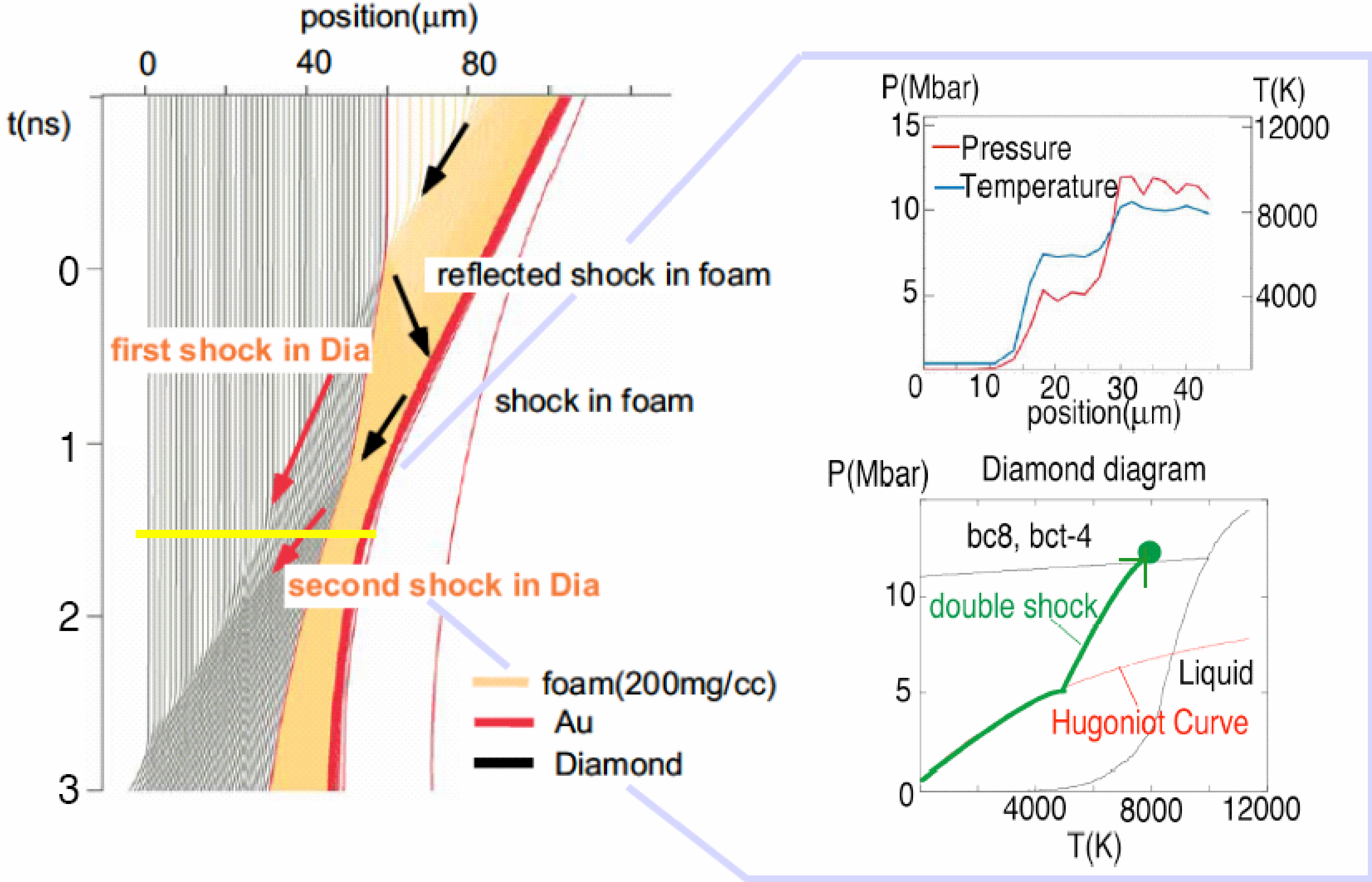

In Warm Dense Matter regime large errors exist even for most studied materials

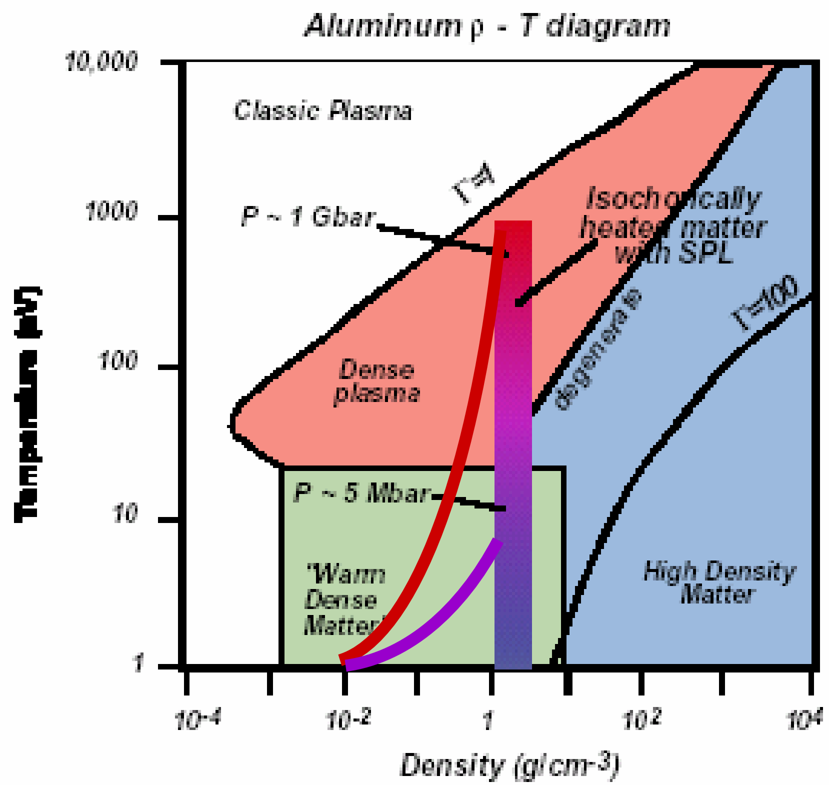

Energetic particles generated UUL can heat the matter rapidly and uniformly to create isochores (ρ is constant) and release isentrops (entropy is constant)

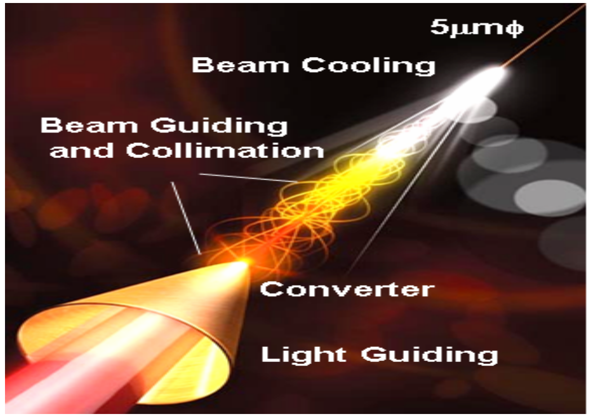

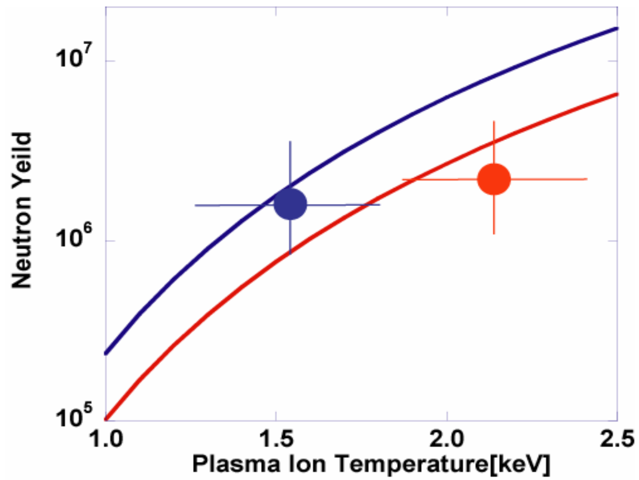

R. Kodama et al., Nature 432,1005,(2004)

爆縮と高速加熱：高密度圧縮と定容加熱

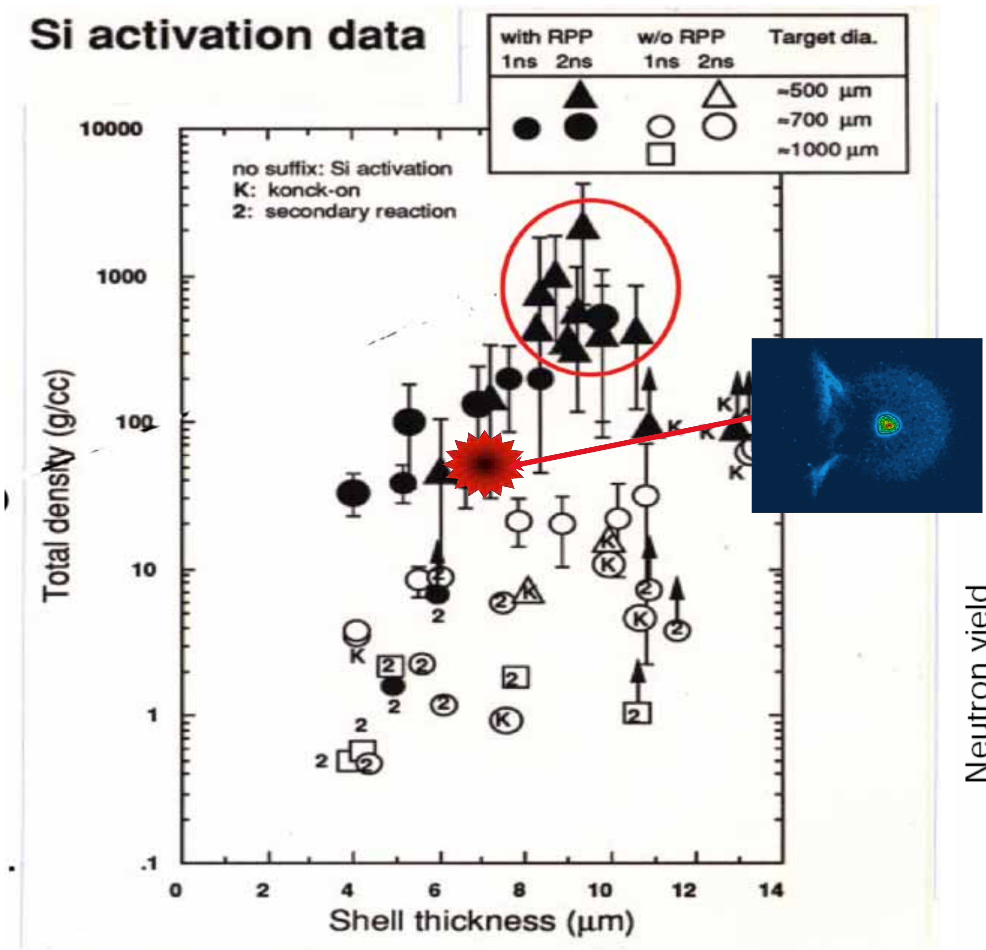

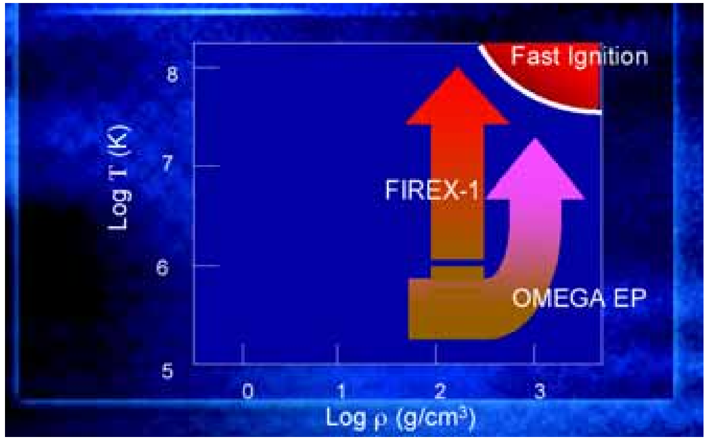

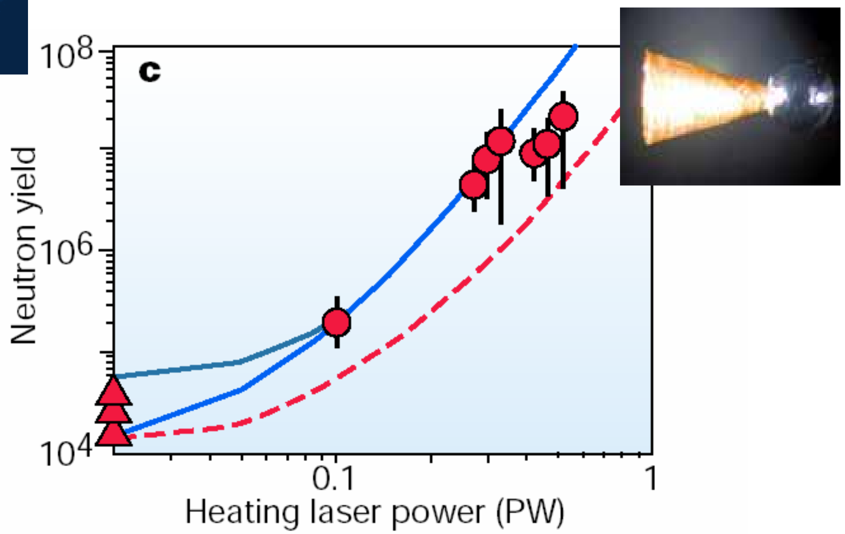

R. Kodama et al., Nature 412, 798 (2001).

R. Kodama et al., Nature 418, 933 (2002).